TURBULENT BOUNDARY LAYER IN AN ADVERSE PRESSURE GRADIENT WITHOUT EFFECT OF WALL CURVATURE*

VICTOR ZAKKAY† AND CHI-RONG WANG††

New York University
University Heights
Bronx, New York 10453

NOVEMBER 1972

---

* The work reported herein was supported by the National Aeronautics and Space Administration under Grant NGR-33-016-181

† Professor of Aeronautics and Astronautics, New York University

†† Research Assistant, New York University

ABSTRACT

An experimental investigation of the hypersonic compressible turbulent boundary layer in an adverse pressure gradient along a cylindrical axisymmetric body has been performed. The tests were conducted in a Mach 6 contoured axisymmetric nozzle. The freestream Reynolds number was 1.24×10^8 per meter and the wall temperature ratio was $T_w/T_{o_\infty} = 0.634$. An external compression cowl was used to produce the gradual adverse pressure gradient. A maximum pressure rise of 7 times the freestream static pressure was achieved in a test region of 23 cm. Boundary layer profiles of static pressure, total pressure, and total temperature, as well as wall transient heat transfer rates, were measured. Comparisons of the velocity total temperature profiles to linear and quadratic relations were made. Measured heat transfer data were in good agreement with the prediction from the flat-plate reference enthalpy method. The integral parameters, when corrected for the normal pressure gradient, were also in good agreement with the results of numerical solutions of the compressible turbulent boundary layer equations.

I. SUMMARY AND INTRODUCTION

Current interest in hypersonic airbreathing propulsion systems utilizing supersonic combustion has stimulated research into turbulent boundary layer behavior under adverse pressure gradient. In order to provide an insight into the fluid flow problem, experimental investigations have been performed and presented in Refs. 1 and 2. These measurements were made in the hypersonic blowdown facility at the Aerospace Laboratory at New York University. In Ref. 1, the adverse pressure gradient was created by a compression flare located in the test section. In Ref. 2, the flare used in Ref. 1, was connected to a streamlined centerbody passing through the nozzle of the same test facility. A thick boundary layer, having thickness of 2.16 cm at the beginning of the compression flare, was obtained. The normal and adverse pressure gradients were created by increasing the radius of curvature of the flare.

In the present experiments, tests were performed in the same wind tunnel facility at New York University. A compression cowl, designed by the inviscid method of characteristics, was used to create an adverse pressure gradient, external to the thick turbulent compressible boundary layer along the cylindrical portion of the centerbody. In this manner, the effect of the radius of curvature of the wall to the boundary layer development was eliminated. Boundary layer profiles of static pressure, total pressure, and total temperature, as well as transient heat transfer rates, were measured. The integral parameters, based on the measured profiles, were computed. Existing theory, presented in Ref. 2, was used to obtain numerical results for comparison to the present experimental results.

II. EXPERIMENTAL APPARATUS

The experiments were performed in the Mach 6 hypersonic blowdown facility at the Aerospace Laboratory at New York University. The stagnation temperature and stagnation pressure for the present tests were 460°K and $1.34 \times 10^7 \frac{\text{Newton}}{m^2}$ respectively. The corresponding freestream Reynolds number was 1.24×10^8 per meter. The wall to total temperature ratio, T_w/T_{o_∞} was 0.634.

The model, shown schematically in Figs. 1 and 2, was a streamlined axisymmetric centerbody passing through the entire length of the nozzle. An axisymmetric cowl with gradual turning angle was inserted into the nozzle to create a longitudinal adverse pressure gradient on the centerbody. The adverse pressure gradient was initiated at a point 158.5 cm downstream from the nozzle throat on the cylindrical portion of the centerbody 11.65 cm in diameter. An initial boundary layer thickness of 2.16 cm was present at this location. The adverse pressure gradient extended downstream for 22 cm, and resulted in a pressure rise of $p_s/p_i = 7.0$. The cylindrical model was equipped with pressure taps and thermocouples to measure the surface distributions of the static pressure and heat transfer rates.

The total pressure, static pressure, and total temperature profiles across the turbulent boundary layer were obtained by traversing the boundary layer from the wall of the centerbody to the external flow with a triple probe, Fig. 3. The probe was also moved in the downstream direction. The static pressure probe has a conical tip faired into a 0.10 cm hypodermic needle. Lateral orifices located 10 to 15 probe diameters downstream were drilled in the probe. The total pressure probe consisted of a hypodermic needle 0.10 cm diameter flattened at the tip with a thickness of 0.015 cm and an opening of 0.005 cm. The total temperature probe was made of an unshield, open-tip chromel-alumel thermocouple.

III. MEASUREMENTS

Profiles of static pressure, total pressure, and total temperature in a distance of 2.5 cm, normal to wall, were measured at eight streamwise positions. Results were tabulated in Tables 1 through 8. A tabulation of the edge Mach number and total pressure at the experimental stations is presented in table 9. The total pressure profiles are shown in Fig. 4. At a distance about 2 cm away from the wall, the total pressure increases and then decreases due to the compression and expansion effects of the cowl. The static pressure profiles are shown in Fig. 5. The normal pressure gradient increases in the streamwise direction. A decrease in the static pressure was found in the last profile. The wall static pressure distribution, Fig. 6, also shows a decrease at the end of the test region. The total temperature profiles are presented in Fig. 7. They do not deviate considerably at different streamwise positions. The Mach number profiles and the velocity profiles are shown in Figs. 8 and 9. The velocity profiles are compared with the 1/7 power velocity law. Comparison of the velocity-total temperature relation to the Crocco linear relation and Walz's quadratic relation, Ref. 3, are shown in Fig. 10. The present test results can be correlated approximately with the Crocco linear relation.

It has been shown in Refs. 4 and 5 that heat transfer rates for turbulent boundary layers in mild adverse pressure gradient were predicted with reasonable accuracy by the Flat-Plate Reference Enthalpy method. The present measurements of the heat transfer rates were compared with the results of the Flat-Plate Reference Enthalpy method in Fig. 11. Satisfactory agreement was also obtained.

IV. INTEGRAL PARAMETERS

Flows with large normal static pressure gradients do not provide a convenient set of reference conditions which can be used to define the boundary layer edge. In Refs. 1 and 2, the boundary layer thickness has been defined as the distance from the wall to the point where the local stagnation pressure differs by 1% from the freestream stagnation pressure. The same method was used to define the boundary layer thickness in the present studies. Measured boundary layer thickness, displacement thickness, and momentum thickness, and the components in the displacement and momentum thickness due to the effects of viscous and normal pressure gradients were computed. Both the inviscid conditions at the edge of the boundary layer and the inviscid wall conditions were used as the reference conditions. Results are shown in Figs. 12 to 16.

Theoretical investigations of the turbulent compressible boundary layer under the effect of adverse pressure gradient have been presented in Ref. 1. This analysis was modified in Ref. 2 to include the effect of the normal pressure gradient, longitudinal adverse pressure gradient, and crossflow in the boundary layer integral equations. This analysis was used to predict the present experiments with zero crossflow effect. Numerical solutions to the integral equations were compared with measurements in Figs. 12 to 16. The distribution of the local skin friction from the numerical solution is shown in Fig. 17.

V. CONCLUSIONS

An experimental investigation of hypersonic axisymmetric turbulent boundary layer in an adverse pressure gradient has been performed. A compression cowl was used to produce a gradual pressure gradient in the absence of longitudinal body curvature. The effect of the longitudinal radius of curvature of the wall along the boundary layer has been eliminated. Boundary layer profiles of static pressure, total pressure, and total temperature at various streamwise locations were measured.

Measurements indicate a characteristic overshoot in the total pressure profiles. Comparison of the present total temperature and velocity relation to the existing total temperature-velocity correlations shows that the present data could be predicted approximately by the linear Crocco relation.

Heat transfer rates increase longitudinally due to the adverse pressure gradient. They are in good agreement with the values predicted by the Flat-Plate Reference Enthalpy Method.

Comparison between the momentum thickness obtained from the numerical solution of the boundary layer integral equation and that obtained from the experiment shows that they are in good agreement. However, some deviations in the boundary layer thickness and displacement thickness between the theory and experiment exist.

REFERENCES

1. Heydysh, W.G. and Zakkay, V., "An Experimental Investigation of Hypersonic Turbulent Boundary Layer in Adverse Pressure Gradient," AIAA Journal, Vol. 7, No. 1, January 1969, pp. 105-116.

2. Zakkay, V., Calarese, W., and Wang, C.R., "A Theoretical and Experimental Investigation of the Hypersonic Turbulent Boundary Layer Subject to Normal and Longitudinal Adverse Pressure Gradients and Cross Flow Along A Windward Plane of Symmetry," AIAA Paper No. 72-187, also will be published as Synoptic in AIAA Journal.

3. Walz, A., "Boundary Layers of Flow and Temperature," The M.I.T. Press, Cambridge, Mass., 1969, p. 115.

4. Zakkay, V. and Callahan, C.G., "Laminar Transitional and Turbulent Heat Transfer to Cone Cylinder Flare Body at Mach 8," Journal of the Aerospace Sciences, Vol. 29, No. 12, December 1962, pp. 1403-1413.

5. Zakkay, V., Bos, A., and Jensen, P.F., Jr., "Laminar Transitional and Turbulent Flow with Adverse Pressure Gradient on a Cone Flare at Mach 10," AIAA Journal, Vol. 5, No. 2, February 1967, pp. 201-207.

6. Miller, L.D., "Predicting Turbulent Compressible Boundary Layers in Strong Adverse Pressure Gradient," J. Spacecraft, Vol. 5, No. 8, August 1968.

$x = 0.00$ cm, $p_{o_\infty} = 1.34 \times 10^{\cdot}$ $\frac{}{m^2}$, T_{o_∞} [illegible]

y(cm)	$p_s \times 10^{-4}$ $\frac{\text{Newton}}{m^2}$	$p_{o_\infty} \times 10^{-4}$ $\frac{\text{Newton}}{m^2}$	T_o ^oK
0.00	0.92	0.92	294
0.13	0.90	5.16	399
0.26	0.88	7.78	424
0.39	0.87	10.00	435
0.52	0.86	11.58	443
0.65	0.86	13.22	447
0.78	0.86	14.93	450
0.91	0.86	17.21	450
1.04	0.86	20.00	450
1.17	0.86	22.60	450
1.3[illegible]	0.86	25.50	450
1.43	0.86	28.20	450
1.56	0.86	30.70	450
1.69	0.86	33.10	450
1.82	0.86	34.80	450
1.95	0.86	36.50	450
2.08	0.86	37.90	450
2.21	0.86	39.30	450
2.34	0.86	39.75	450
2.47	0.86	39.90	450

Table 1 Data of pressure and temperature measurements

$x = 3.81$ cm, $\quad p_{O_2\infty} = 1.34 \times 10^7 \frac{\text{Newton}}{m^2}$, $\quad T_{O\infty} = 455^{o}K$

y(cm)	$p_s \times 10^{-4} \frac{\text{Newton}}{m^2}$	$p_{O_2} \times 10^{-4} \frac{\text{Newton}}{m^2}$	T_o ^{o}K
0.00	1.65	1.65	294
0.13	1.65	9.64	401
0.26	1.62	11.7	409
0.39	1.51	15.1	420
0.52	1.27	15.8	428
0.65	1.34	20.6	433
0.78	1.45	26.2	439
0.91	1.45	32.4	446
1.04	1.41	37.2	450
1.17	1.38	45.5	455
1.30	1.34	53.7	455
1.43	1.38	57.2	455
1.56	1.34	57.2	455
1.69	1.38	57.2	455
1.82	1.38	57.6	455
1.95	1.41	59.3	455
2.08	1.38	58.5	455
2.21	1.27	56.5	455
2.34	1.20	55.8	455
2.67	1.17	56.1	455

Table 2 Data of pressure and temperature measurements

$x = 6.98$ cm, $p_{o\infty} = 1.34 \times 10^{-4} \frac{\text{Newton}}{m^2}$, $T_{o\infty}$ [illegible]

y(cm)	$p_s \times 10^{-4} \frac{\text{Newton}}{m^2}$	$p_{o2} \times 10^{-4} \frac{\text{Newton}}{m^2}$	T_o °K
0.00	2.20	2.20	294
0.13	2.14	13.10	394
0.26	2.10	15.40	406
0.39	2.00	18.80	417
0.52	1.96	22.85	425
0.65	1.93	28.55	433
0.78	1.89	36.40	441
0.91	1.86	44.40	449
1.04	1.62	54.40	451
1.17	1.58	65.10	451
1.30	1.72	71.70	451
1.43	1.65	70.30	451
1.56	1.58	68.90	451
1.69	1.55	68.20	451
1.82	1.55	68.20	451
1.95	1.55	70.30	451
2.08	1.58	71.70	451
2.21	1.58	70.90	451
2.34	1.48	6 .80	451
2.47	1.34	65.50	451

Table 3 Data of pressure and temperature measurements

x = 10.16 cm, $p_{o\infty} = 1.34 \times 10^{7} \frac{\text{Newton}}{m^2}$, $T_{o\infty} = 456^{o}K$

y(cm)	$p_s \times 10^{-4} \frac{\text{Newton}}{m^2}$	$p_{o2} \times 10^{-4} \frac{\text{Newton}}{m^2}$	T_o ^{o}K
0.00	2.93	2.93	294
0.13	2.93	15.15	400
0.26	2.89	20.00	412
0.39	2.75	24.80	424
0.52	2.55	33.10	431
0.65	2.55	41.30	441
0.78	2.44	52.35	449
0.91	2.44	66.90	455
1.04	2.52	83.40	459
1.17	2.48	89.50	459
1.30	2.38	88.90	459
1.43	2.20	84.05	459
1.56	2.00	79.90	459
1.69	2.00	81.30	459
1.82	1.93	78.50	459
1.95	1.86	77.10	459
2.08	1.79	76.40	459
2.21	1.76	77.10	459
2.34	1.76	77.90	459
2.47	1.79	79.10	459

Table 4 Data of pressure and temperature measurements

y(cm)	$p_s \times 10^{-4}$ $\frac{\text{Newton}}{m^2}$	$p_{o2} \times 10^{-4}$ $\frac{\text{Newton}}{m^2}$	T_o ^oK
0.00	3.38	3.38	294
0.13	3.28	20.65	412
0.26	3.30	26.20	418
0.39	3.17	34.40	426
0.52	3.10	44.10	435
0.65	3.03	59.90	444
0.78	2.96	80.60	453
0.91	2.90	92.35	458
1.04	2.72	95.00	458
1.17	2.58	94.40	458
1.30	2.55	94.40	458
1.43	2.55	93.70	458
1.56	2.41	92.40	458
1.69	2.20	91.60	458
1.82	2.06	87.50	458
1.95	1.93	87.50	458
2.08	1.93	86.10	458
2.21	1.79	82.00	458
2.34	1.72	77.80	458
2.47	1.65	77.20	458

Table 5 Data of pressure and temperature measurements

$x = 16.26$ cm, $p_{o\infty} = 1.34 \times 10^{7} \frac{\text{Newton}}{m^2}$, $T_{o\infty} = 458^{o}K$

y (cm)	$p_s \times 10^{-4} \frac{\text{Newton}}{m^2}$	$p_{o2} \times 10^{-4} \frac{\text{Newton}}{m^2}$	T_o ^{o}K
0.00	4.20	4.20	294
0.13	4.13	31.00	417
0.26	3.99	39.90	425
0.39	3.86	48.90	435
0.52	3.75	68.90	439
0.65	3.72	83.40	452
0.78	3.72	08.90	460
0.91	3.68	117.00	463
1.04	3.62	116.30	463
1.17	3.10	114.20	463
1.30	3.31	111.60	463
1.43	3.35	109.40	463
1.56	2.96	104.00	463
1.69	2.68	99.10	463
1.82	2.65	96.50	463
1.95	2.51	91.50	463
2.08	2.20	84.00	463
2.21	1.86	75.00	463
2.34	1.79	70.90	463
2.47	1.62	64.00	463

Table 6 Data of pressure and temperature measurements

$x = 19.05$ cm, $p_{o\infty} = 1.34 \times 10^{7} \frac{\text{Newton}}{m^2}$, $T_{o\infty} = 458^{o}K$

y(cm)	$p_s \times 10^{-4} \frac{\text{Newton}}{m^2}$	$\rho_{o2} \times 10^{-4} \frac{\text{Newton}}{m^2}$	T_o ^{o}K
0.00	5.41	5.41	294
0.13	5.17	31.70	407
0.26	5.17	39.30	417
0.39	4.82	48.90	424
0.52	4.61	61.30	432
0.65	4.31	84.00	440
0.78	4.00	99.85	447
0.91	3.85	113.00	450
1.04	3.76	116.30	450
1.17	3.65	114.20	450
1.30	3.58	112.20	450
1.43	3.41	108.20	450
1.56	3.17	104.80	450
1.69	2.89	97.10	450
1.82	2.68	92.95	450
1.95	2.52	89.50	450
2.08	2.27	82.70	450
2.21	2.06	77.10	450
2.34	1.96	73.00	450
2.47	1.79	67.50	450

Table 7 Data of pressure and temperature measurements

$x = 21.84$ cm, $\quad p_{o\infty} = 1.34 \times 10^{7} \frac{\text{Newton}}{\text{m}^2}$, $\quad T_{o\infty} = 450^{o}K$

y(cm)	$p_s \times 10^{-4} \frac{\text{Newton}}{\text{m}^2}$	$p_{o2} \times 10^{-4} \frac{\text{Newton}}{\text{m}^2}$	T_o ^{o}K
0.00	4.83	4.83	294
0.13	4.62	42.05	418
0.26	4.79	46.85	424
0.39	4.31	60.00	428
0.52	4.20	70.95	439
0.65	4.17	82.00	443
0.78	4 13	97.85	453
0.91	4.07	108.90	457
1.04	4.00	114.30	458
1.17	3.86	111.60	458
1.30	3.62	107.50	458
1.43	3.31	100.70	458
1.56	3.03	95.80	458
1.69	2.86	91.60	458
1.82	2.68	89.60	458
1.95	2.55	85.40	458
2.08	2.38	82.00	458
2.21	2.20	77.90	458
2.34	2.00	72.40	458
2.47	1.83	66.15	458

Table 8 Data of pressure and temperature measurements

x cm	M_e	$P_{o2} \times 10^{-4} \frac{\text{Newton}}{m^2}$	$P_{01} \times 10^{-4} \frac{\text{Newton}}{m^2}$	P_{01} / P_{t_∞}
0.00	6.00	38.4	1293	0.965
3.81	5.60	57.2	1460	1.088
6.98	5.35	61.7	1306	0.975
10.16	4.90	83.4	1252	0.935
13.34	4.80	92.3	1281	0.955
16.26	4.60	110.0	1310	0.970
19.05	4.60	110.0	1310	0.970
21.84	4.60	114.3	1350	1.006

TABLE 9

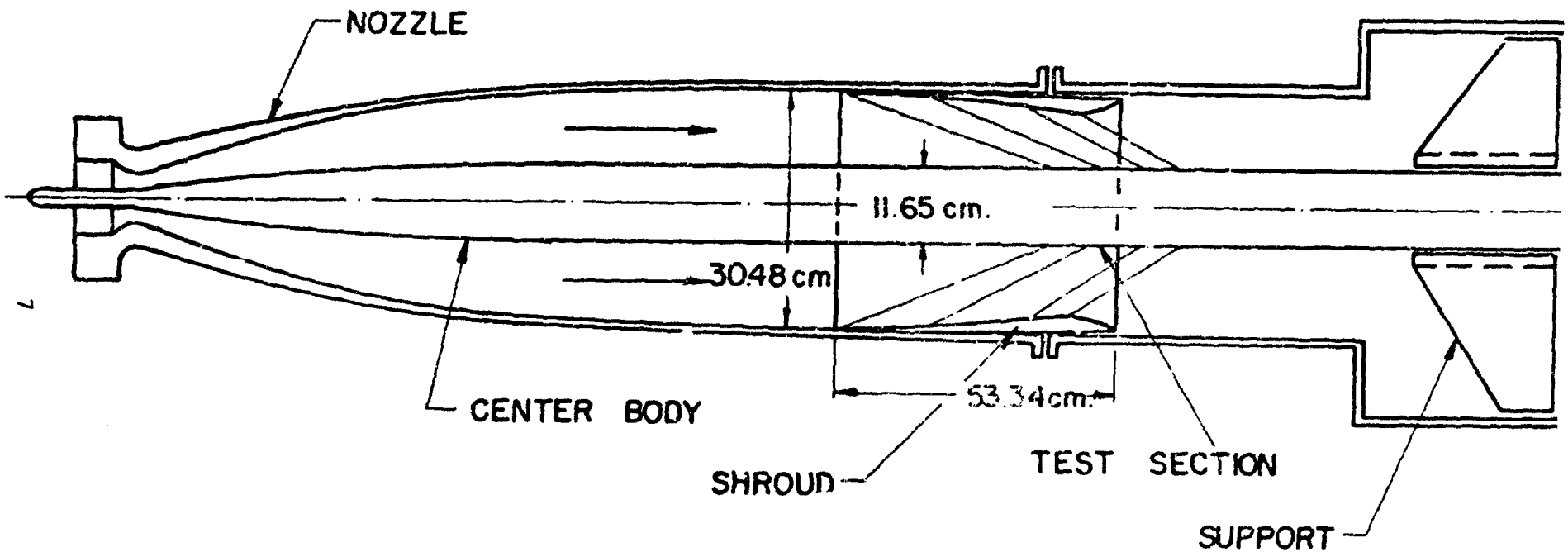

Fig. 1 Schematic of Wind Tunnel Setup

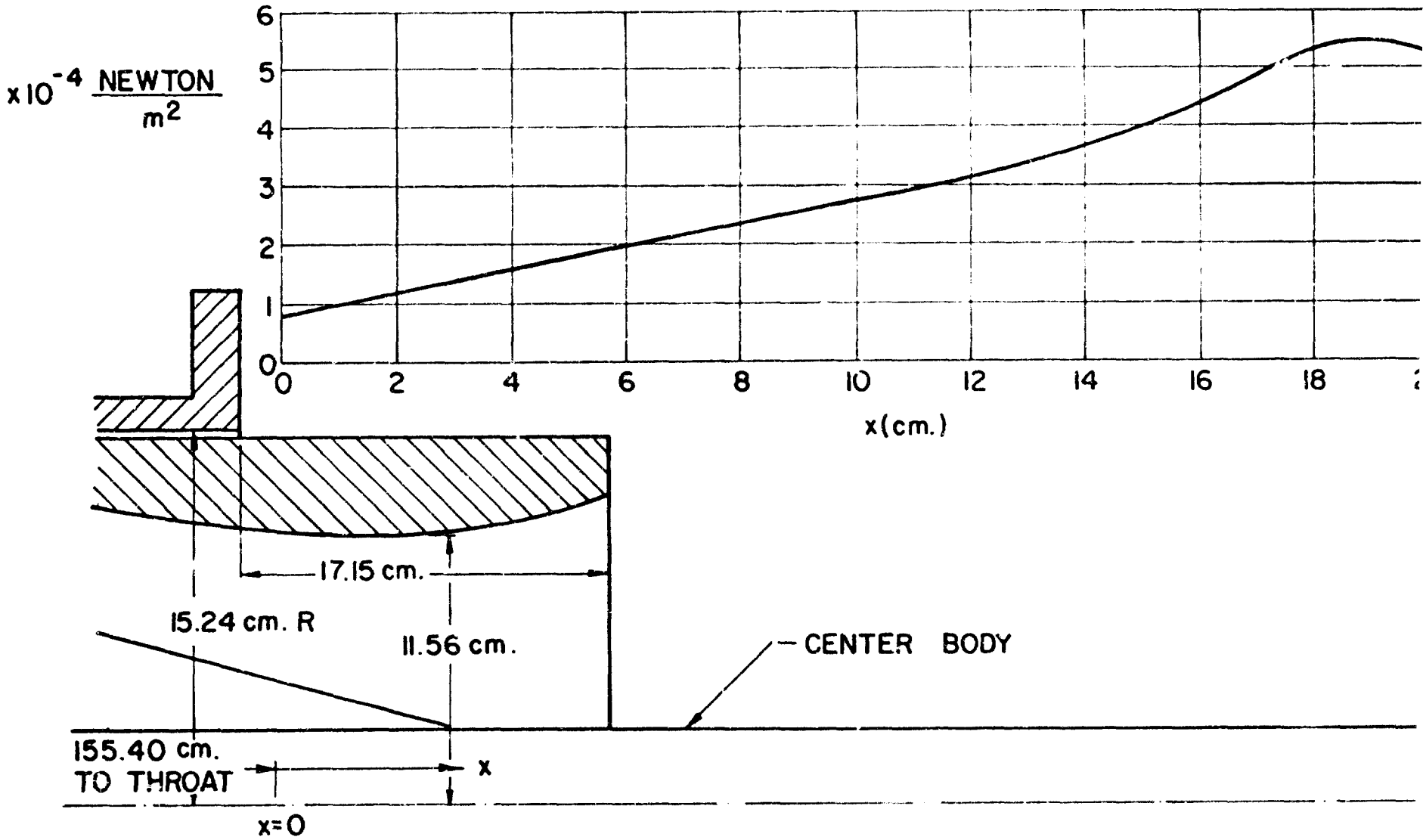

Fig. 2 Schematic of test region

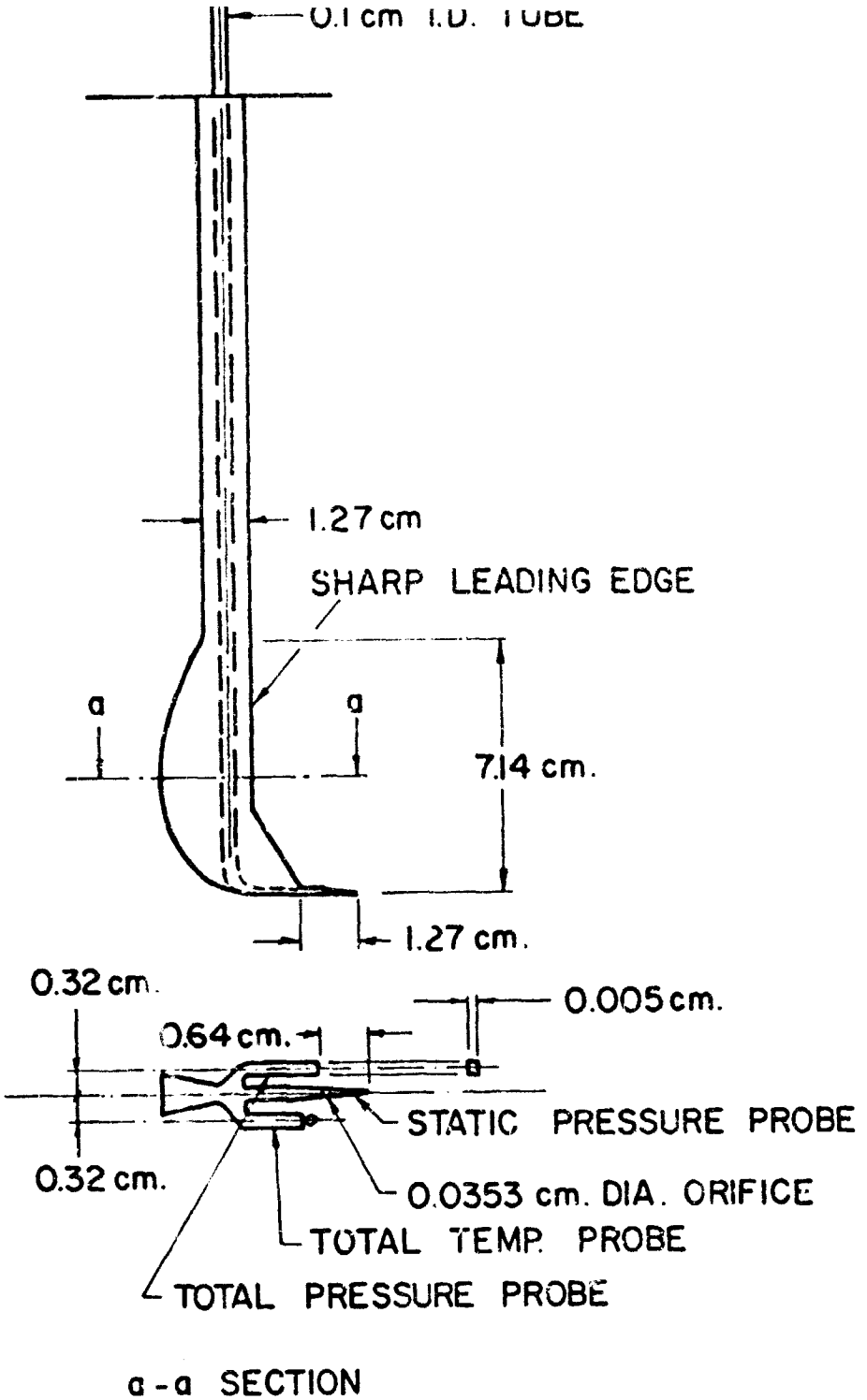

Fig. 3 Schematic of triple probe

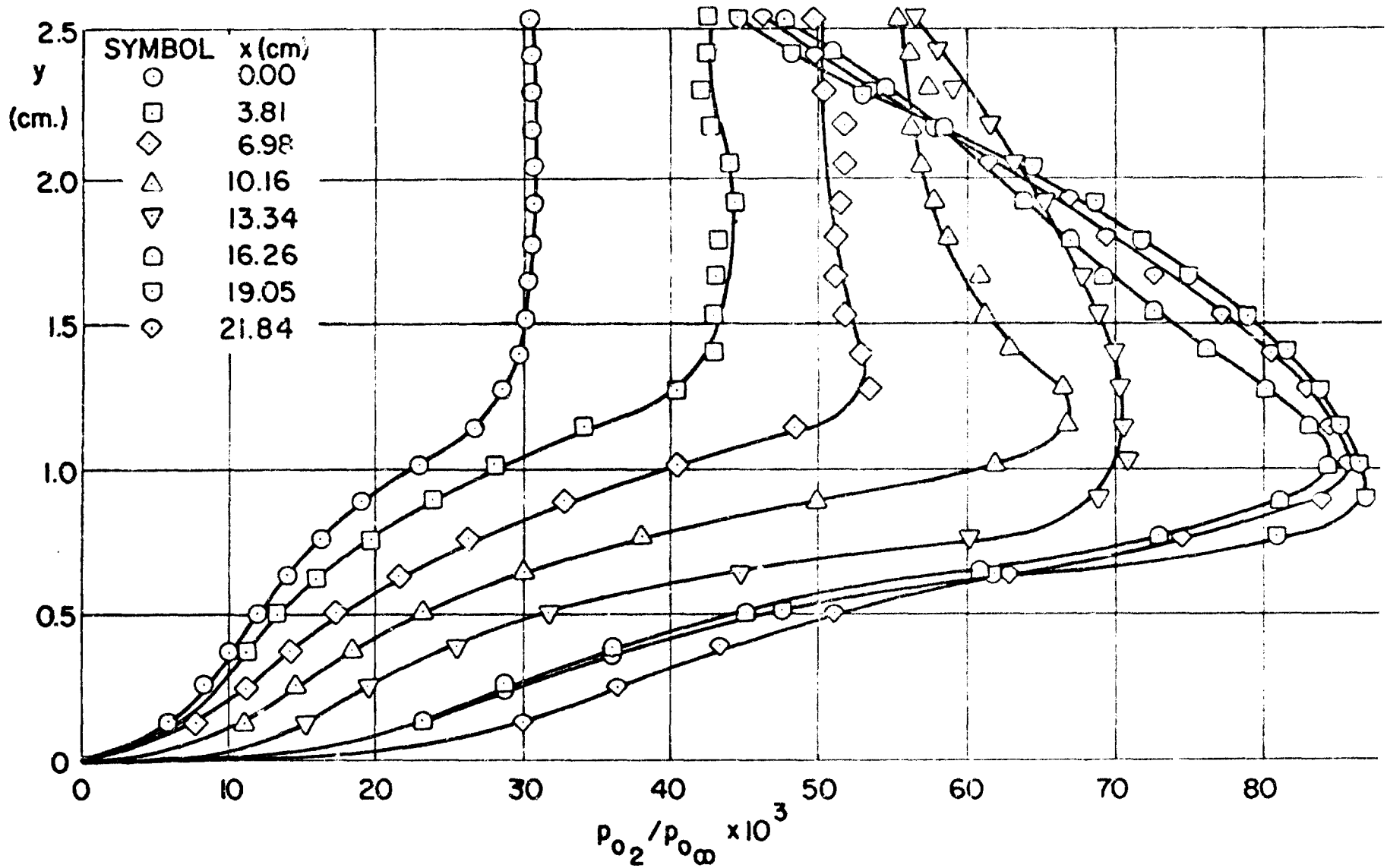

Fig. 4 Total pressure profiles

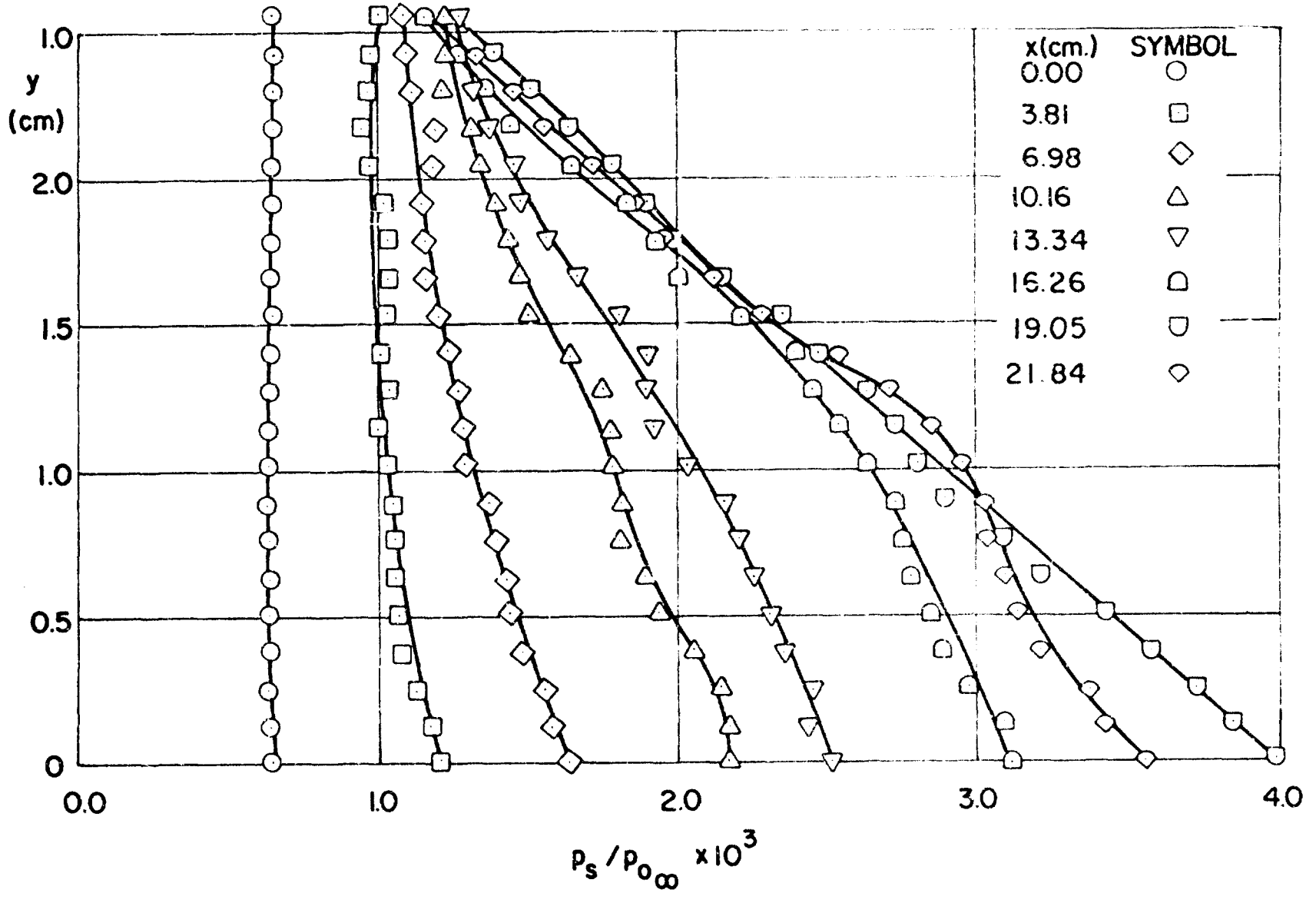

Fig. 5 Static pressure profiles

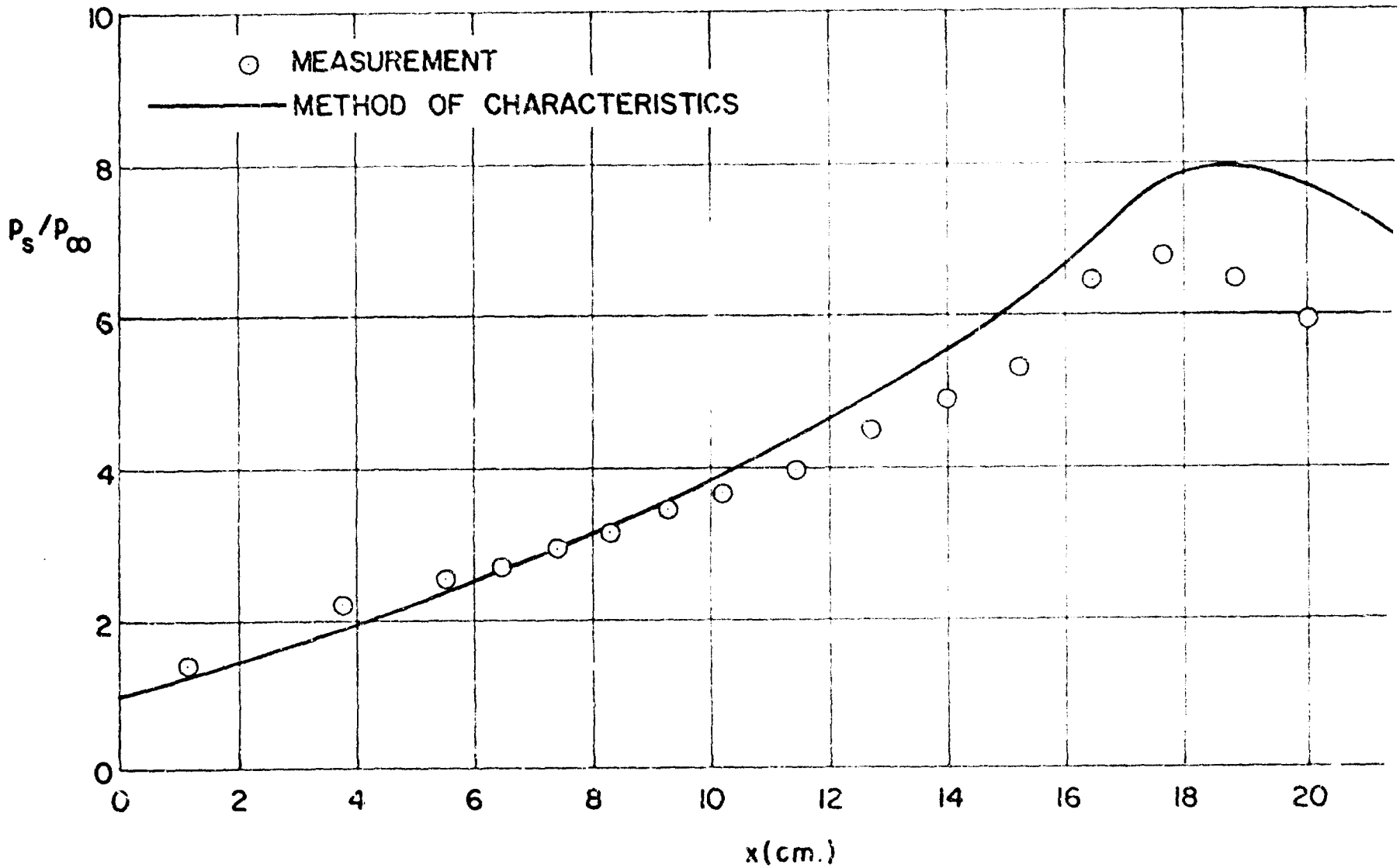

Fig. 6 Distribution of wall static pressure

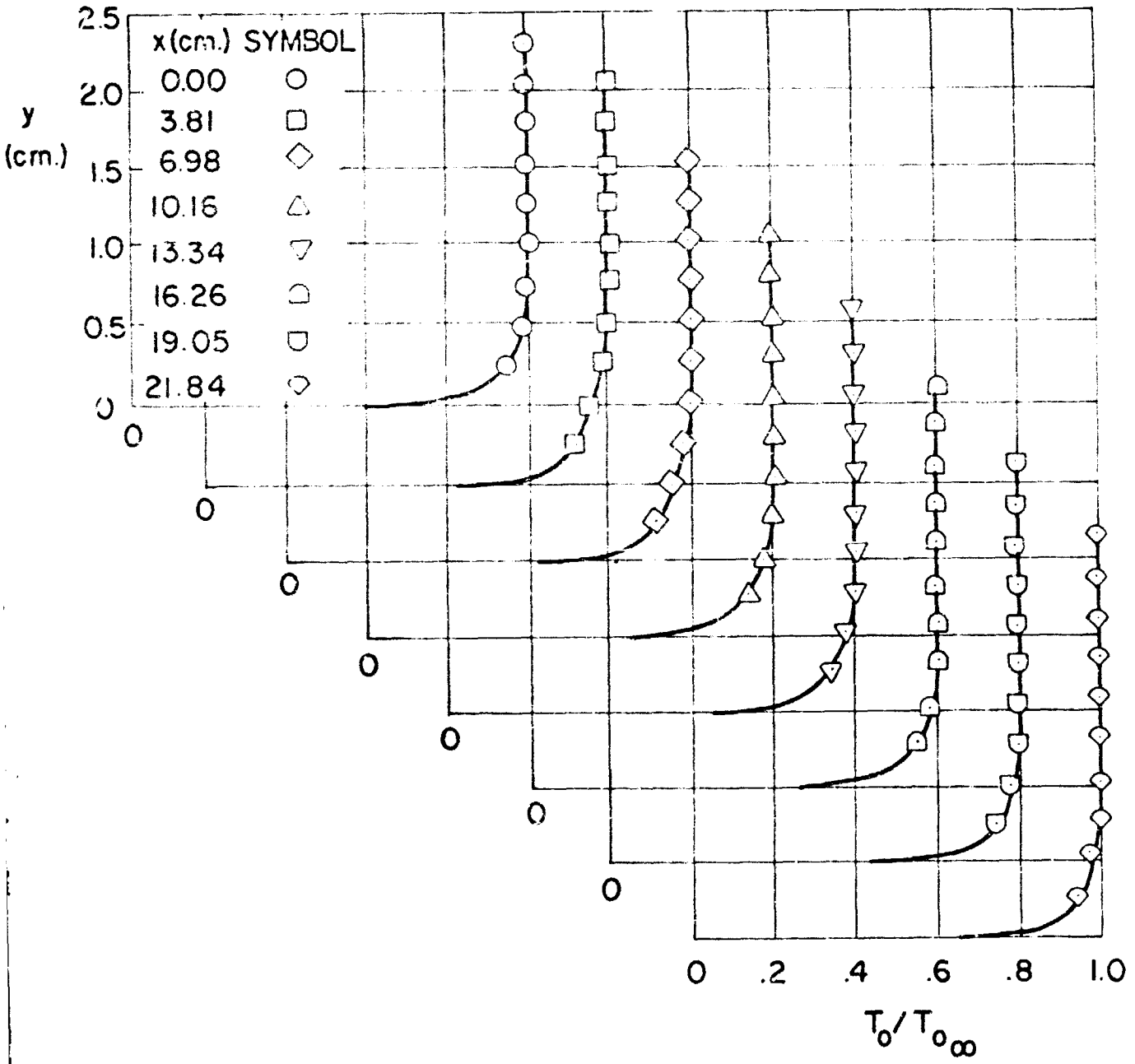

Fig. 7 Measured total temperature profiles

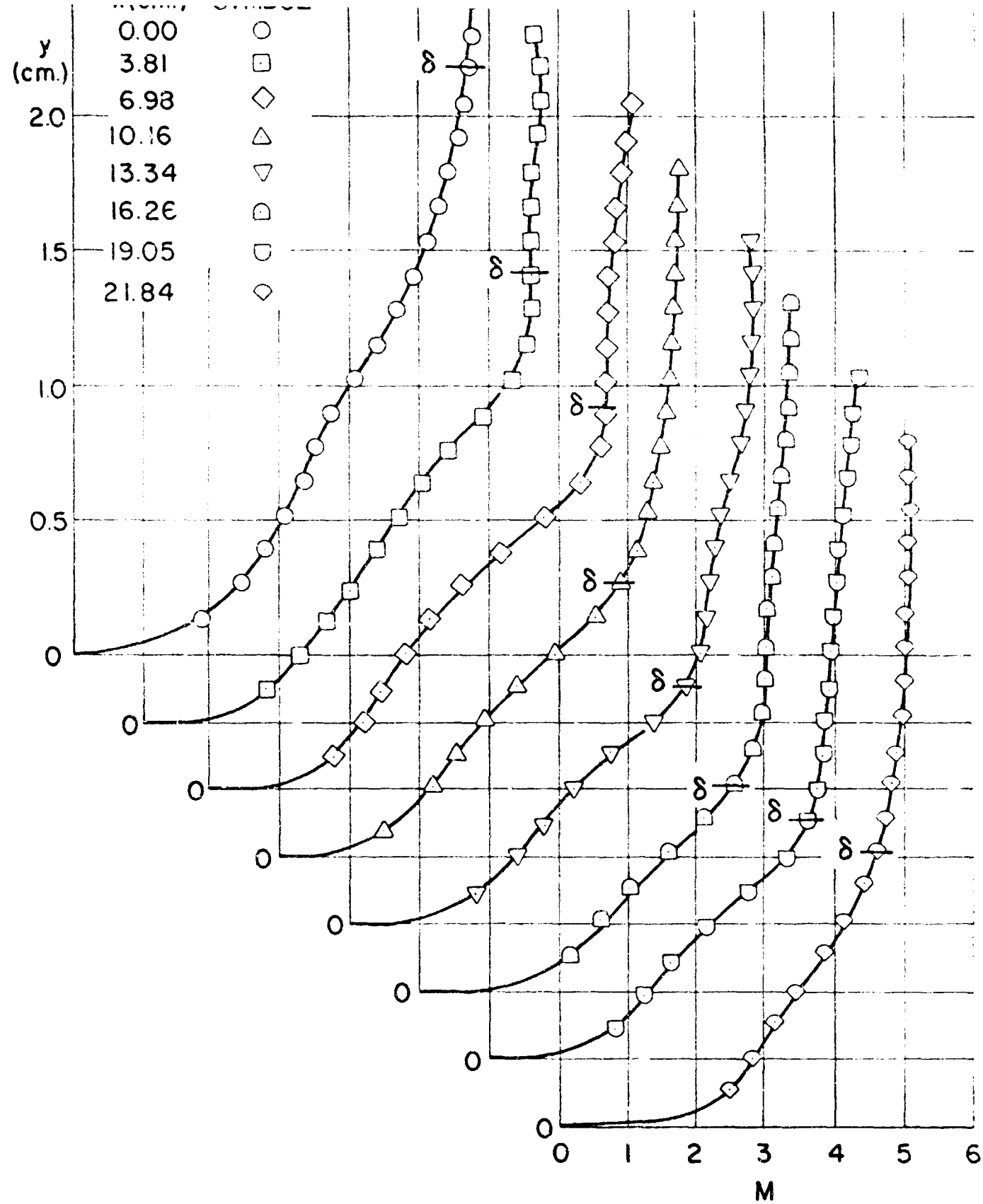

Fig. 8 Mach number profiles

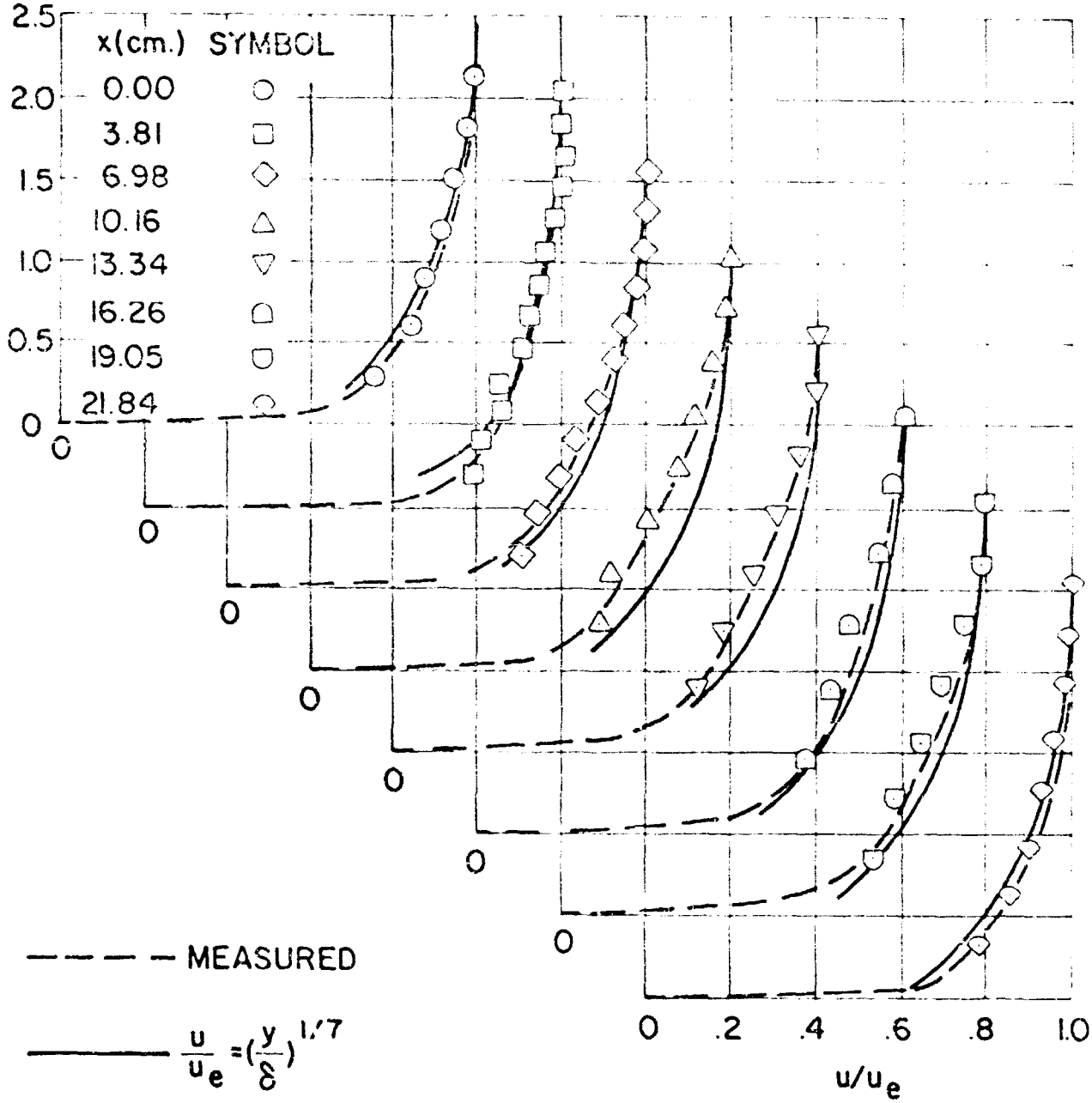

Fig. 9 Velocity profiles

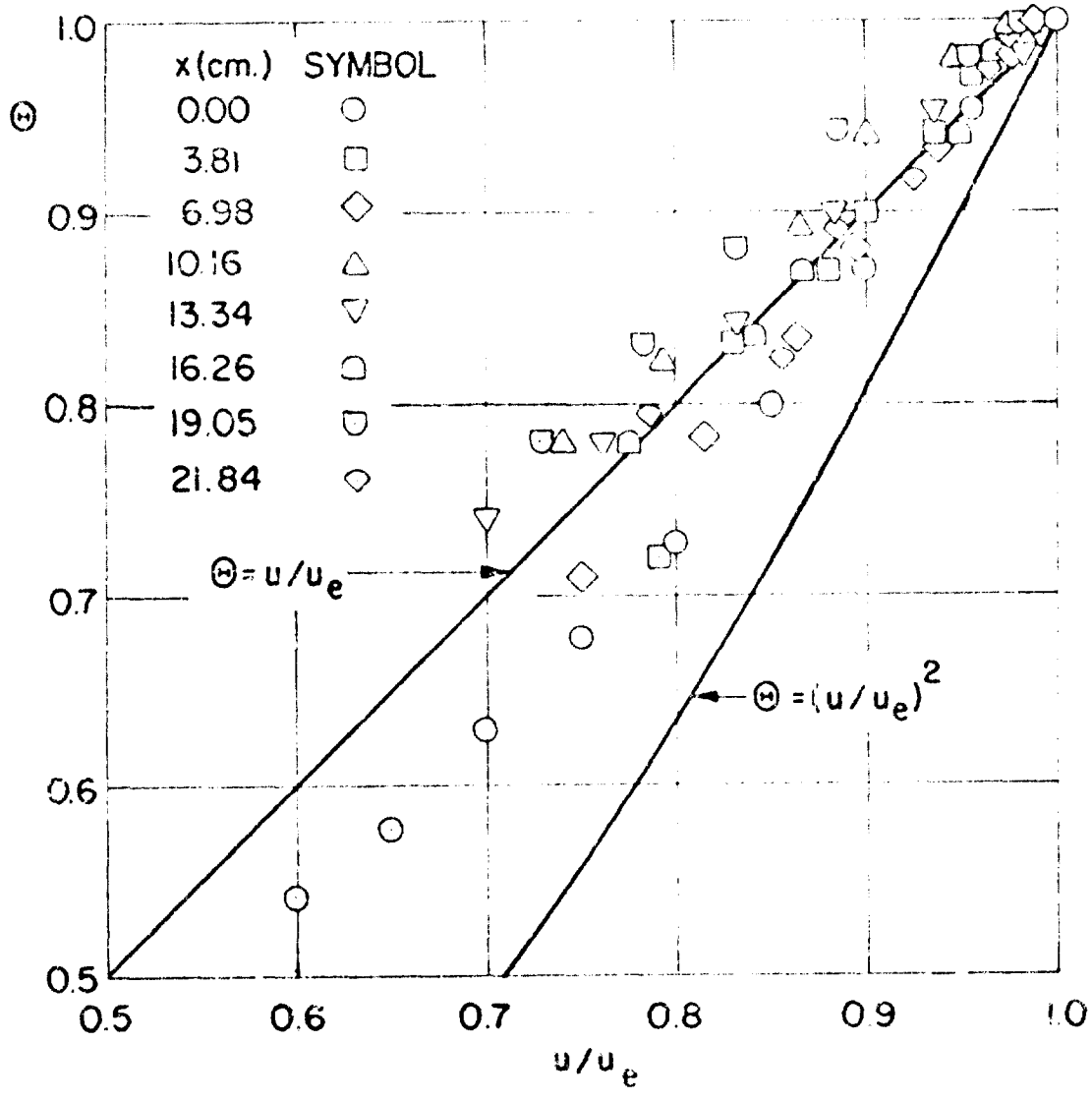

Fig. 10 Comparison of velocity-total temperature profile to linear and quadratic relationship

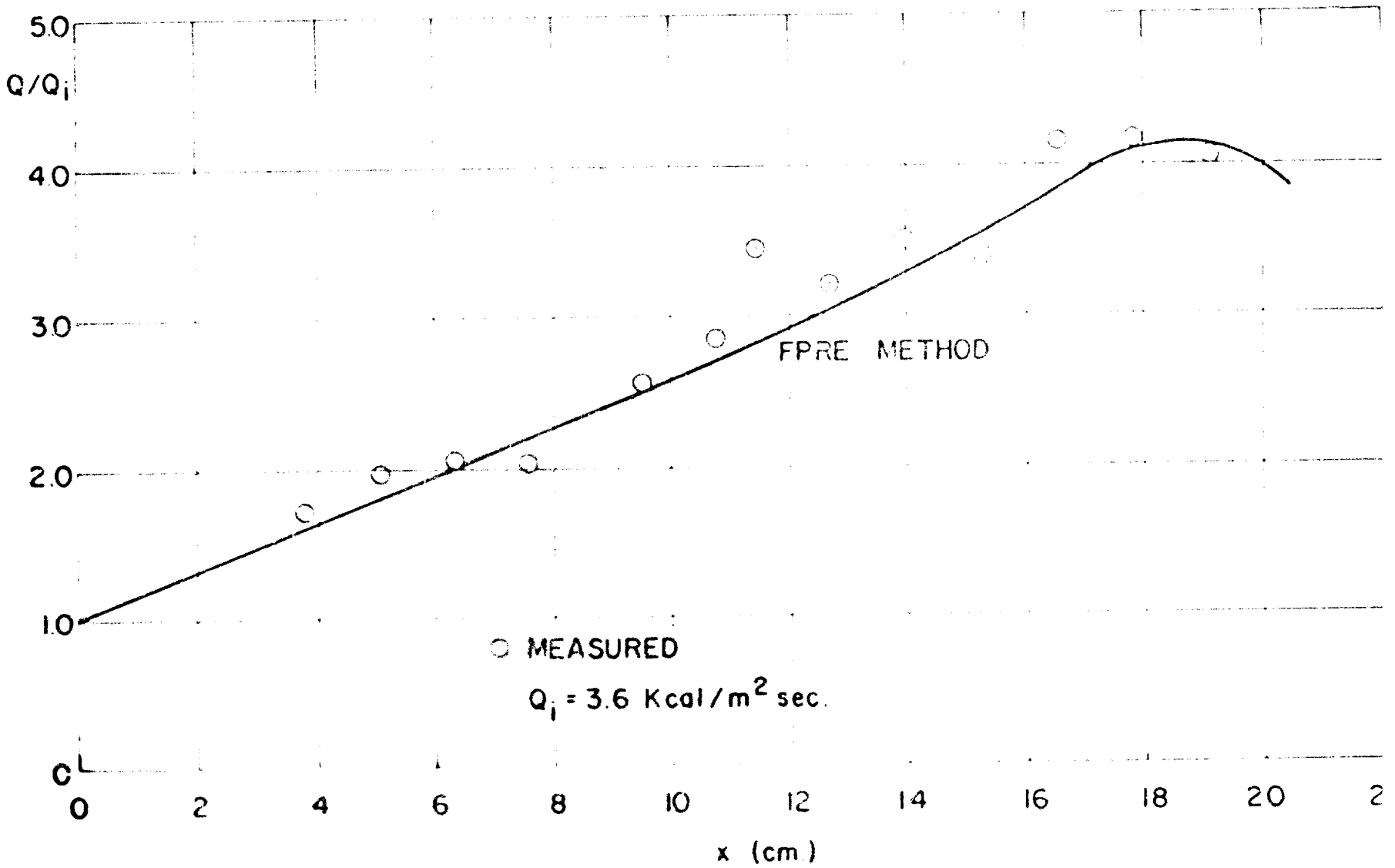
5.0
Q/Q_i
4.0
3.0
2.0
1.0
0
2
4
6
8
10
12
14
16
18
20
FPRE METHOD
MEASURED
Q_i = 3.6 Kcal/m^2 sec.
x (cm)

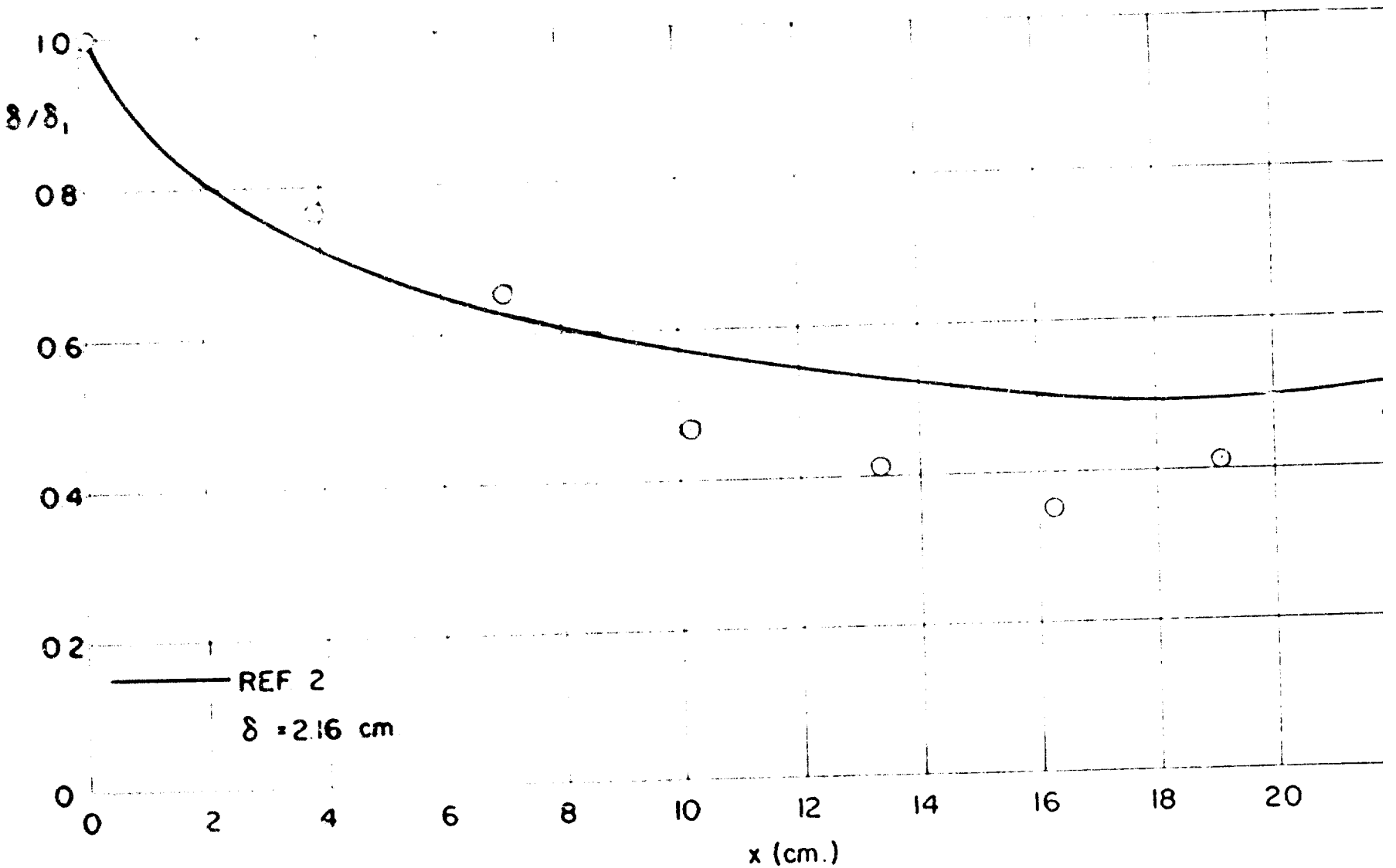

Fig. 12 Correlation of boundary layer thickness

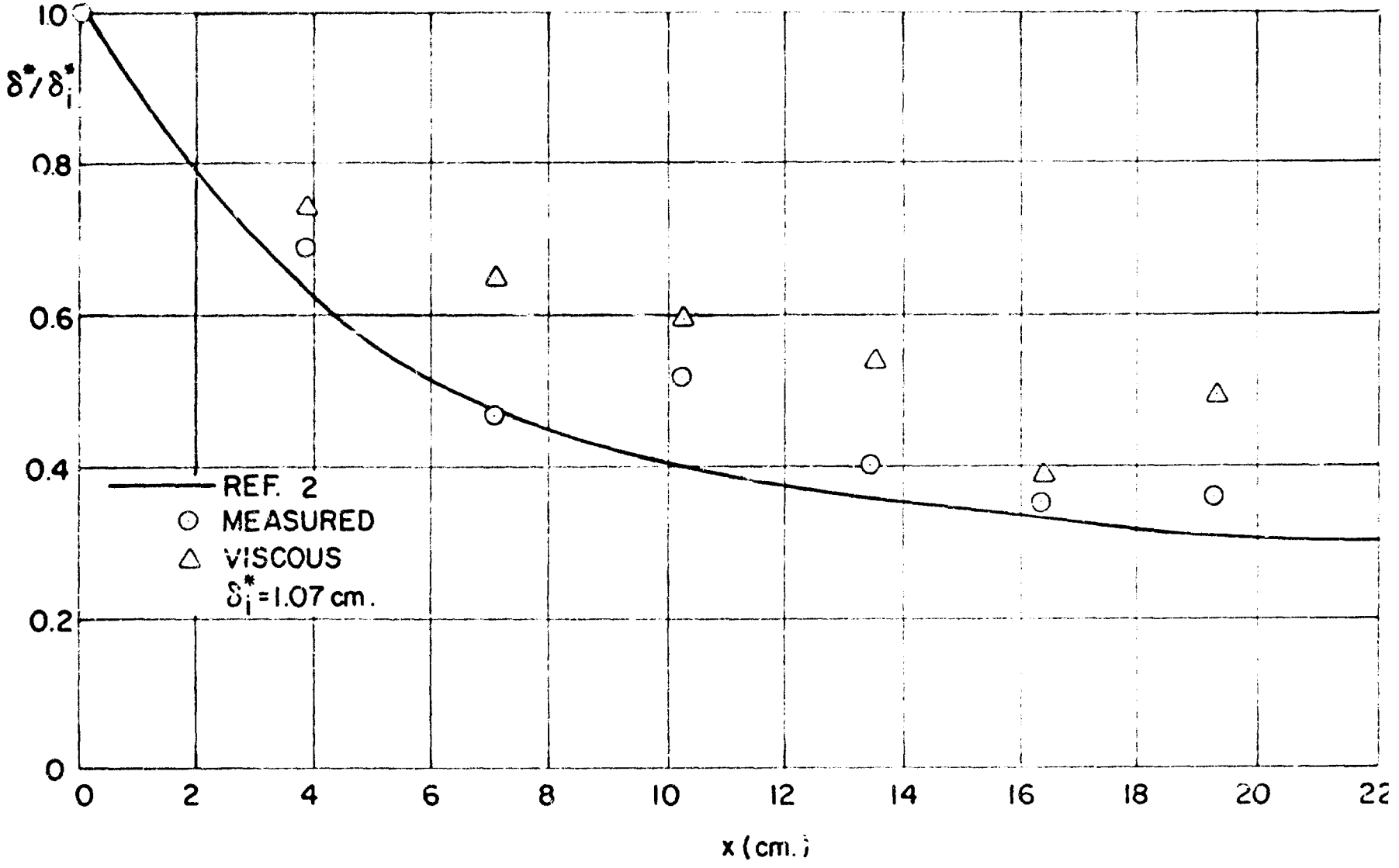

Fig. 12 Distribution of displacement thickness based on the edge conditions

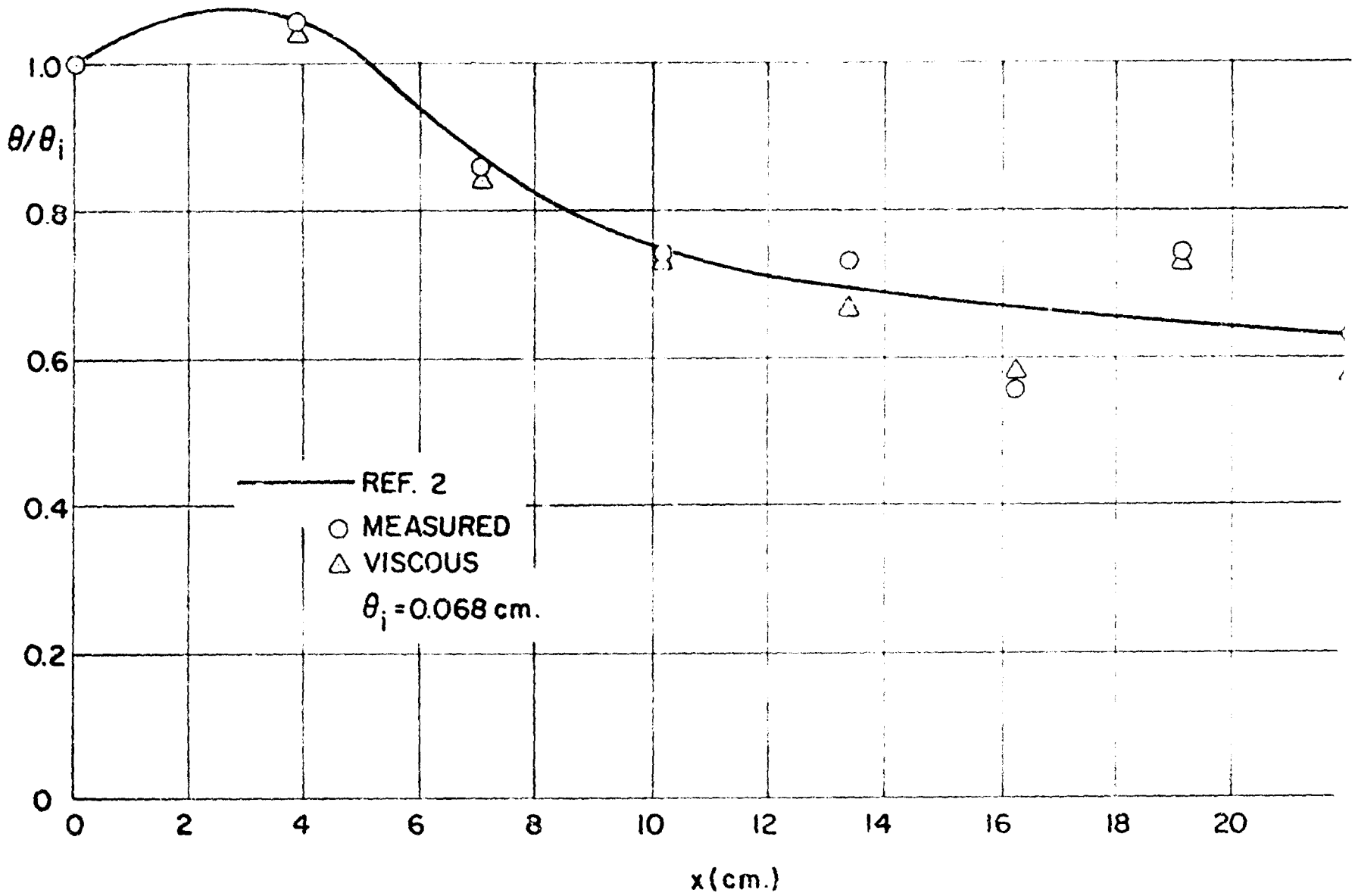

Fig. 14 Distribution of momentum thickness based on the edge conditions

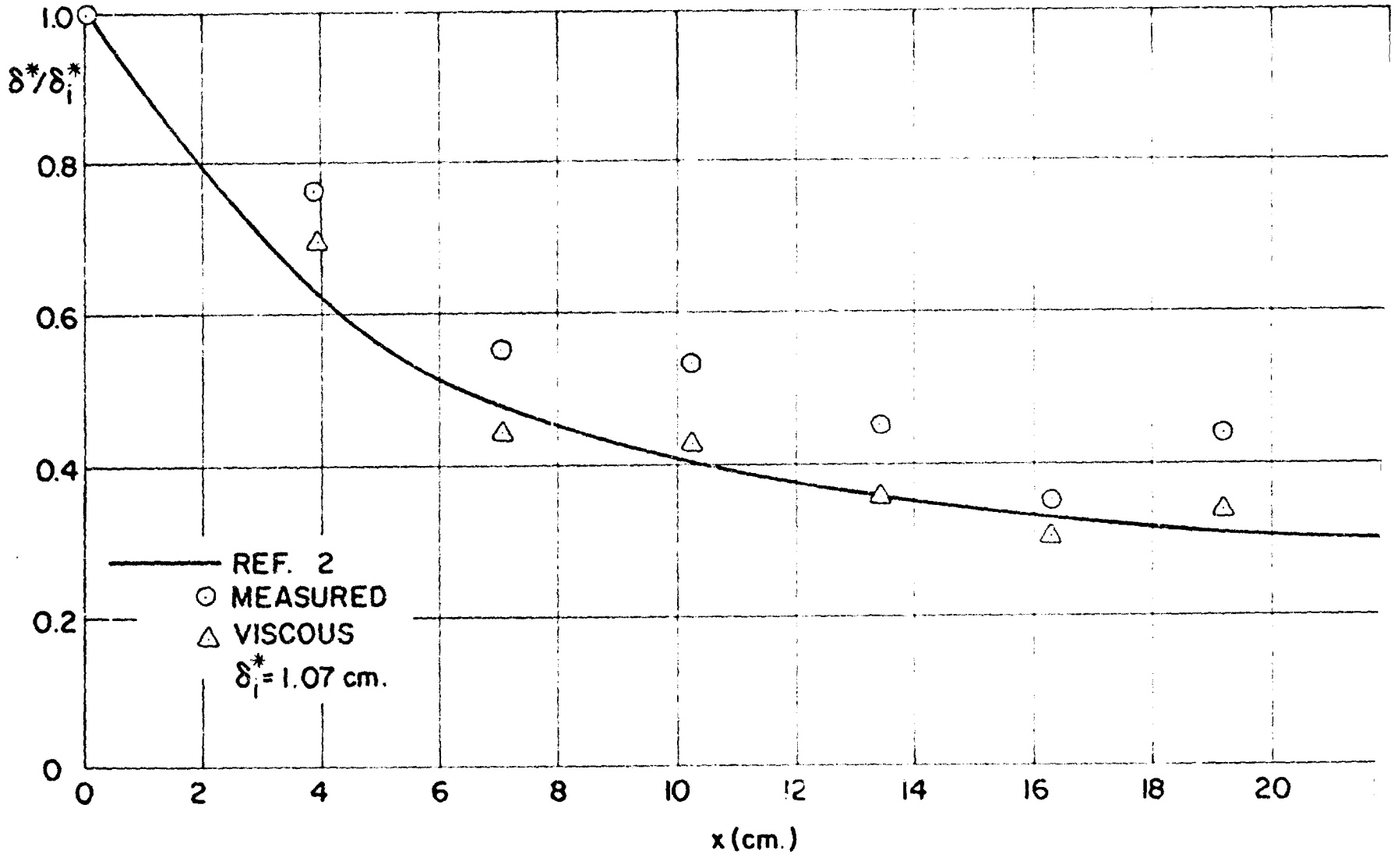

Fig. 15 Distribution of displacement thickness based on wall conditions

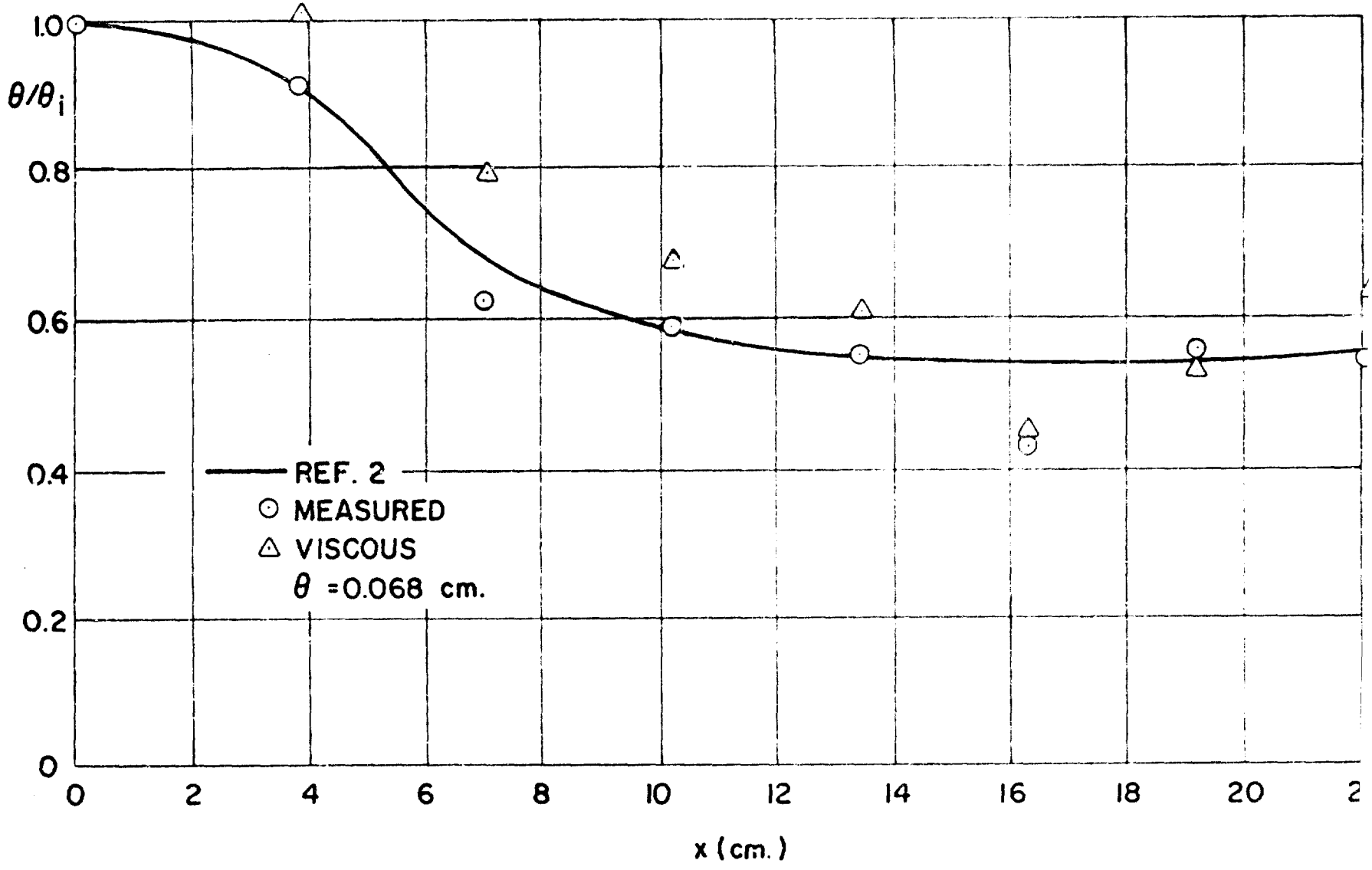

Fig. 16 Distribution of momentum thickness based on wall conditions

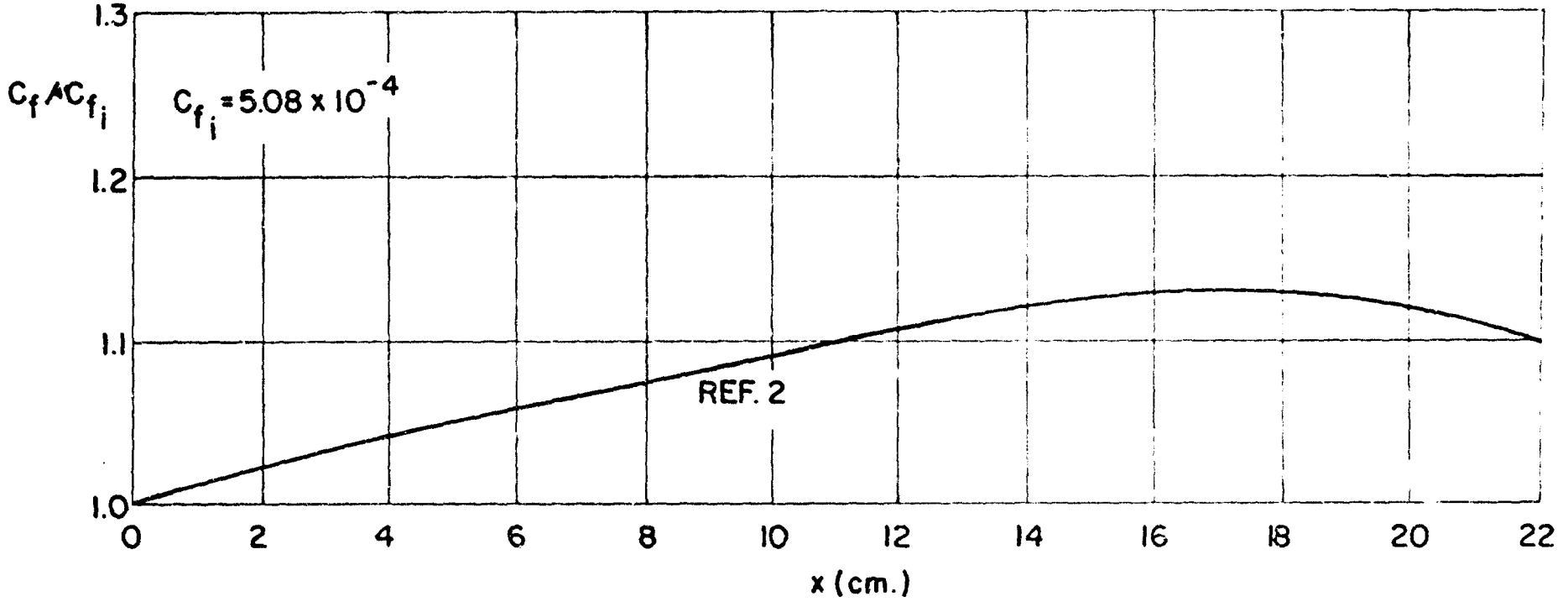

Fig. 17 Distribution of skin friction